Appl Phys B (2010) 99: 13–17
DOI 10.1007/s00340-010-3951-8

Applied Physics B
Lasers and Optics

RAPID COMMUNICATION

Highly birefringent soft glass rectangular photonic crystal fibers with elliptical holes

R. Buczynski · I. Kujawa · D. Pysz · T. Martynkien · F. Berghmans · H. Thienpont · R. Stepien

Received: 13 October 2009 / Revised version: 22 January 2010 / Published online: 10 March 2010

Abstract In this paper we report on the fabrication of highly birefringent photonic crystal fiber with a photonic cladding composed of elliptical holes ordered in a rectangular lattice. The fiber features a group birefringence G of 0.82×10^{-4} at 725 nm. We discuss the influence of structural parameters including the ellipticity of the air holes and the aspect ratio of the rectangular lattice on the birefringence and on the modal properties of the fiber.

1 Introduction

It is well known that photonic crystal fibers (PCFs) can exhibit much higher birefringence values than their conventional counter parts such as *bow tie* and *panda* type optical fibers. In the latter the birefringence stems from mechanical stresses induced in the core. Fibers with an elliptical cross-section also exhibit birefringence as a result of the broken axial symmetry of the structure. In PCFs the birefringence results from the asymmetric distribution of the effective refractive index in the fiber cross-section. This distribution depends on the hole lattice type, as well as on the size and on the spatial distribution of the holes [1–3]. A typical PCF which has three-fold rotational symmetry, for example, with an ideal hexagonal lattice and circular holes, is not birefringent [4]. Examples of fibers with high birefringence values have been reported for applications in sensing and in telecommunications [5, 6].

In this paper we focus on the challenging task of producing PCFs with elliptical holes. The properties of these PCFs attracted substantial interest of several groups, which resulted in a number of theoretical papers [7–16]. Steel and Osgood [7] predicted high birefringence levels around 10^{-2} in silica PCFs with elliptical holes arranged in a hexagonal lattice, where the structure has twofold symmetry. Further work focused on optimizing structural parameters and on taking into account the modal properties and the attenuation of the fundamental mode [8–10]. This resulted in a design of an elliptical hole PCF with low attenuation in the range 0.1–10 dB/km and high phase birefringence 3.7×10^{-2} [11]. The influence of a small central hole on the PCF properties was also studied [12, 13]. PCFs with elliptical holes and a rectangular lattice were then found to have higher birefringence since the lattice enhances the total fiber anisotropy [14, 15]. Further work underlined the possibility of dispersion shaping with those types of structures [16].

Whereas such particular structures undoubtedly feature interesting and useful characteristics, their fabrication remains very challenging. Elliptical holes with controlled dimensions are indeed much more difficult to obtain than circular holes. A successful demonstration of a polymer PCF with elliptical holes made from polymethyl methacrylate (PMMA) using an extrusion method was reported by Issa et al. [17]. This polymer PCF exhibited a birefringence on

R. Buczynski (✉)
Faculty of Physics, University of Warsaw, Pasteura 7,
02-093 Warsaw, Poland
e-mail: rbuczyns@igf.fuw.edu.pl
Fax: +48-22-5546822

R. Buczynski · I. Kujawa · D. Pysz · R. Stepien
Glass Laboratory, Institute of Electronic Materials Technology,
Wolczynska 133, 01-919 Warsaw, Poland

T. Martynkien
Institute of Physics, Wroclaw University of Technology,
Wybrzeze Wyspianskiego 27, 50-370 Wroclaw, Poland

F. Berghmans · H. Thienpont
Department of Applied Physics and Photonics, Vrije Universiteit
Brussel, Pleinlaan 2, 1050 Brussels, Belgium

the order of 10^{-4} at 850 nm. We also reported earlier on attempts to fabricate soft glass PCFs with elliptical holes using a stack and draw technique. The obtained structures were however irregular, and their low quality prevented adequately characterizing the fibers [15].

In this letter we deal with our latest achievements in the fabrication of elliptical hole PCFs with rectangular lattice. First, we briefly describe the fabrication process. Second, we deal with the measurement set-up and with our experimental results. Finally, we compare these results with our simulations. To the best of our knowledge, it is the first time that successful fabrication of photonic crystal fiber with regular lattice of elliptical holes in glass can be reported.

2 Fabrication

The lattice geometry used at the PCF preform stage influences the shape of the air-holes formed during the fiber drawing process [18]. One typically observes the tendency to form air-holes with a shape that matches the lattice geometry. This effect can be controlled for structures with a high air filling factor. Choosing a rectangular lattice at the preform stage therefore results in elliptical air-holes during drawing of the subpreform (Fig. 1). However, during fiber drawing, the subpreform air-holes tend to become circular, which renders controlling the elliptical hole features very difficult.

We nevertheless succeeded to manufacture the PCF with a cross-section depicted in Fig. 1. Our fiber counts five rings of elliptically shaped holes. To specify the structure, we rely on the following definitions: the lattice constant along the X-axis Λ_x; the lattice constant along the Y-axis Λ_y; the lattice constant ratio $\rho = \Lambda_y/\Lambda_x$; the ellipticity of the air holes $\eta = d_x/d_y$, where d_x and d_y represent the minor and major axis of the air-filled ellipse, and the linear filling factors f_x and f_y given by

$$f_a = \frac{d_a}{\Lambda_a}, \quad a \in X, Y. \tag{1}$$

The lattice constants of our fiber are $\Lambda_x = 2.0$ µm and $\Lambda_y = 5.1$ µm. The size of the elliptical holes varies slightly depending on the location in the structure (Fig. 1c). The holes have a minor and major axes $d_x = 350$ nm and $d_y = 700$ nm, respectively, yielding linear filling factors of $f_x = 0.18$ and $f_y = 0.14$ (Fig. 1d).

The base material for our PCF is a borosilicate glass labeled NC-21A. This multicomponent glass is synthesized in-house at ITME and has an oxide composition detailed in Table 1. This glass is selected to verify our stack and draw technology for elliptical holes fabrication. The main physical properties of NC21A are: refractive index $n_D = 1.533$, density $\rho = 2.50$ g/cm^3, coefficient of thermal expansion

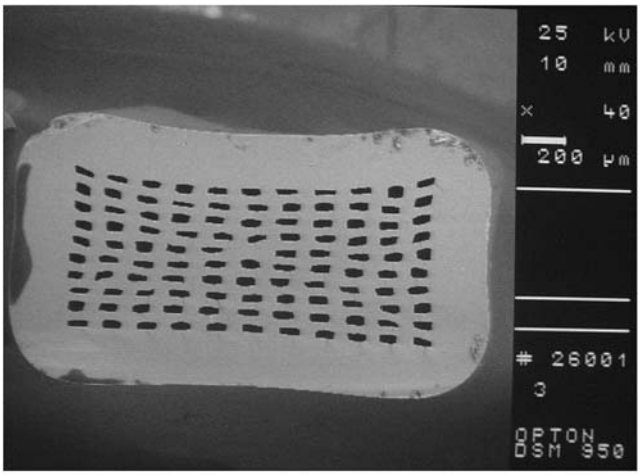

a

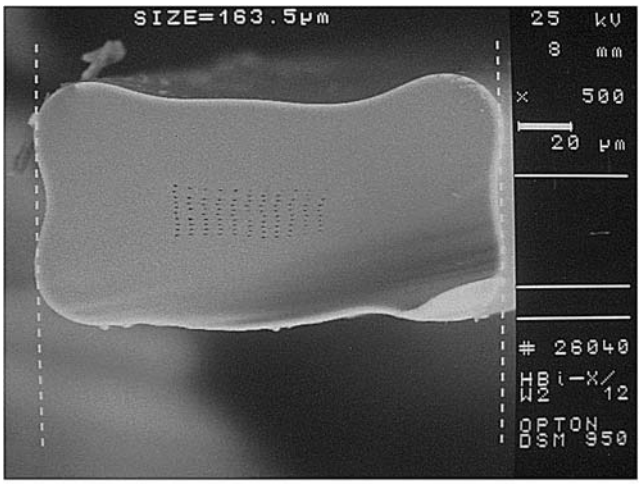

b

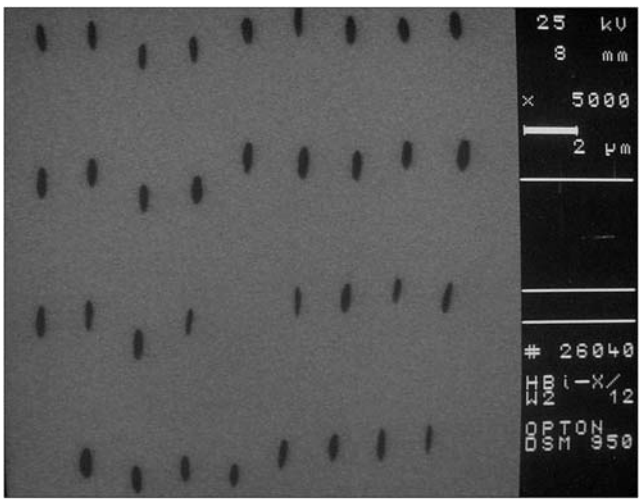

c

Fig. 1 Subpreform with rectangular air-holes (**a**), PCF drawn from this subpreform (**b**), PCF cladding with elliptical holes (**c**), typical shape of the elliptical holes (**d**)

d

Fig. 1 (*Continued*)

Table 1 Oxide composition of borosilicate NC-21A glass

SiO_2	Al_2O_3	B_2O_3	Li_2O	Na_2O	K_2O	As_2O_3
55.0	1.0	26.0	−3.0	9.5	5.5	0.8

$\alpha_{20\text{–}300} = 82 \times 10^{-7}$ K^{-}1, glass transition temperature $T_g =$ 500°C and softening point $D_{\mathrm{TM}} = 530$°C.

The transmission of NC-21A glass is limited to the range 380–2700 nm with a relatively high attenuation of 4 dB/m. We measured an attenuation of more than 6 dB/m for our PCF, which is a result of this high attenuation of borosilicate glass itself and of the relatively low filling factor of the structure.

For the preform fabrication, we use ellipse-like capillaries with axis aspect ratio of 0.5 and linear filling factors of $f_x = 0.2$ and $f_y = 0.1$ ordered in rectangular lattice. A core of the fiber is formed with a single elliptical rod. During subpreform and fiber drawing, we use a low-speed drawing process to ensure homogenous heat distribution in the subpreform and a relatively low pulling temperature of 720°C to preserve the ellipticity of the air holes. The drawing process is performed on 6-m-long fiber drawing tower. We use a feeding speed of 1.2 mm/min, while the pulling speed is 0.5 m/min. Adjusting those drawing parameters is essential to obtain elliptical holes. For our final fiber, we intentionally chose a rectangular cross section (Fig. 1b) which allows easily identifying the main axis and avoiding twisting of the fiber in the measurement set-ups.

3 Measurement results

The parameters characterizing the birefringence properties of birefringent PCF are the phase birefringence B defined as the difference between the propagation constants β_x and β_y of the two orthogonally polarized components HE_{11x} and HE_{11y} of the fundamental mode:

$$B = n_x - n_y = \frac{\lambda}{2\pi}(\beta_x - \beta_y), \tag{2}$$

and the group birefringence G defined as

$$G = -\frac{\lambda^2}{2\pi L}\frac{d\Delta\phi}{d\lambda}. \tag{3}$$

B and G are different for PCF, while they are almost the same for conventional fiber [19]. We used the spectral interferometric method with crossed polarizers to determine the group birefringence. The interferometer is shown in Fig. 2.

Polarized supercontinuum light obtained with a highly nonlinear PCF pumped with a femtosecond Ti:Sapphire laser is launched into our fiber. A first polarizer is aligned so that both polarization modes were equally excited. At the output of our fiber, an analyzer is oriented at 90° with respect to the input polarizer. The output signal is registered using a spectrum analyzer and monitored with a CCD camera. The CCD camera allows verifying proper light coupling into the core of the PCF. The spectrum analyzer records the modulation of the intensity as a function of wavelength, which results from the interference between the polarized components of the propagating mode. Maximum intensity occurs when

$$\frac{d\Delta\phi}{d\lambda} = \pm 2\pi, \tag{4}$$

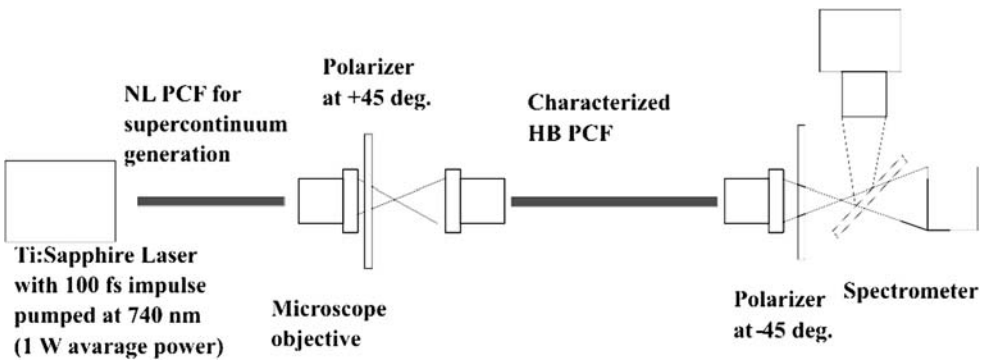

Fig. 2 Group birefringence measurement set-up

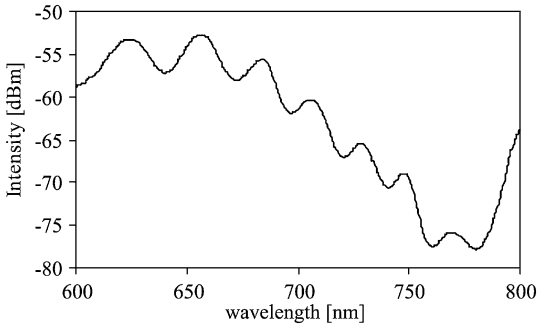

Fig. 3 Measurement of group birefringence using the spectral method with a supercontinuum source. The measured interferogram shows interference between polarization components in the PCF at 45° with respect to its main axis. Measurements are performed for a PCF length of 325 mm with a supercontinuum source pumped at 800 nm

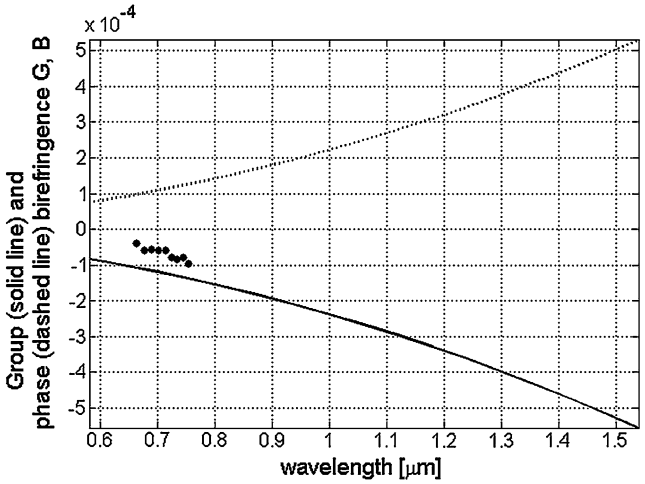

Fig. 4 Calculated group (G) and phase (B) birefringence for the fabricated fiber structures based on the actual fiber structure. *Circles* represent measured values of group birefringence obtained with supercontinuum source pumped at 800 nm

where $\Delta\phi$ is the phase shift corresponding to successive fringes in the output spectrum represented by their maxima, and $\Delta\lambda$ is the distance between successive fringes.

The group birefringence given by (2) can then be calculated as

$$|G| = \frac{\lambda^2}{\Delta\lambda L}, \tag{5}$$

where λ is an average wavelength between two successive fringes, and L is the length of the measured fiber.

A measurement interferogram is depicted in Fig. 3. Based on this interferogram, the group birefringence can be calculated using (4) and (5) as depicted in Fig. 4. We have obtained a group birefringence modulus of $G = 0.82 \times 10^{-4}$ at 725 nm. The sign of G cannot be directly determined in our experiment; however, modeling returns a negative sign for G.

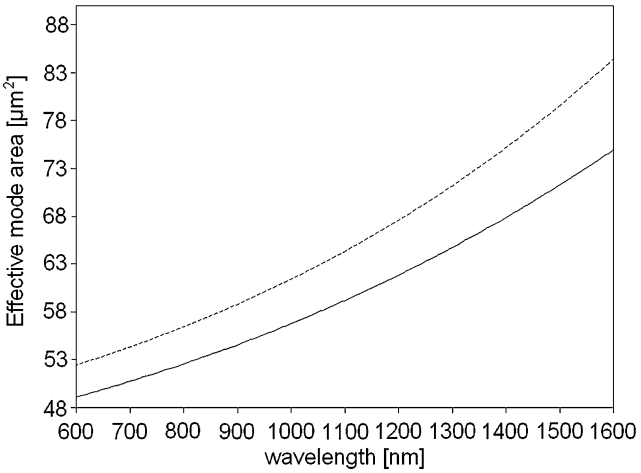

Fig. 5 The effective mode area of the fundamental mode for both polarization (*solid line*—X-polarized mode and *dashed line*—Y-polarized mode) as a function of wavelength

Using in-house software based on a plane wave expansion method [20], we calculated the phase and group birefringence using the actual structural parameters as obtained from an SEM photograph (Fig. 1). We took into account the material dispersion of NC21 glass. The calculated values presented in Fig. 4 are in fairly good agreement with the measured group birefringence values. Differences between modeling and experimental values stem from the limited resolution and threshold level of binarized SEM photograph used for modeling.

According to numerical simulations of the actual fiber, the confinement losses of higher modes are at least one order of magnitude higher than for the fundamental mode. Therefore, in practice this fiber can be treated as a single mode one. The calculated effective mode area for fundamental mode is about 52 μm^2 at wavelength 700 nm. The effective mode area as a function of wavelength is presented in Fig. 5.

The fabricated fiber has a regular structure with high aspect ratio of the elliptical holes. However we observe some irregularities in distribution and size of the air holes (Fig. 1c), which results in asymmetry of mode patterns (Fig. 6). The filling factor of the fiber is low (0.18 and 0.14); therefore, mode fields are distributed widely around defect core area, which results in relatively low birefringence.

Further improvement of the fiber parameters is possible with decrease of the lattice pitch and increase of filling factor for similar aspect ratio of elliptical holes. It will result in larger value of birefringence. As shown by the simulations, if we decrease the lattice pitch by 50% and double the filling factor, the phase birefringence of the fiber will increase significantly (up to 4.1×10^{-3} at 700 nm). A dramatic improvement of the fiber attenuation will also be achieved by replacing the borosilicate glass (NC21) with a high-quality low-attenuation silicate glass.

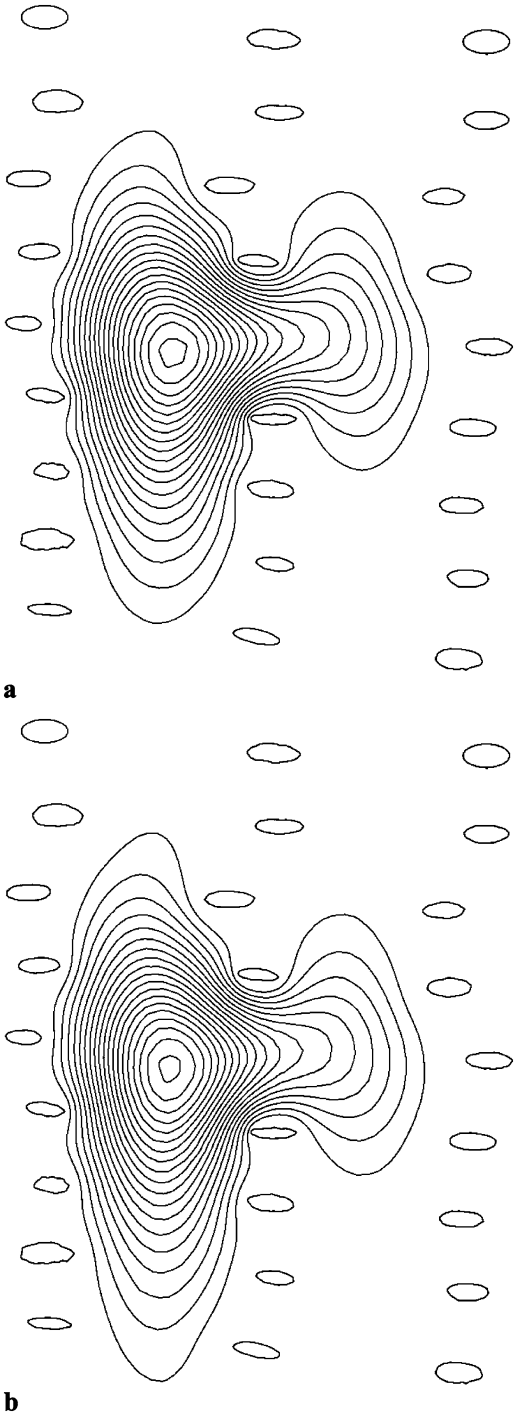

Fig. 6 Contour maps of the field intensity distribution at wavelength 700 nm for—X-polarized (**a**) and—Y-polarized (**b**) mode

4 Conclusion

We have shown that it is possible to fabricate a glass PCF with elliptical holes. These holes are arranged in a rectangular lattice. The phase birefringence is on the order of 10^{-4} due to the low air filling factor, and the group birefringence reached values of $G = 0.82 \times 10^{-4}$ at 725 nm. These PCFs can find applications in optical fiber directional transverse strain sensors with the benefit that their rectangular cross-section allows avoiding twist during mounting and provides straightforward orientation of the polarization axis with respect to the direction of applied force.

Acknowledgements This work was supported in part by Polish Ministry of Science and Information Society Technologies grant NN515244737, by the COST 299 action, and by an internal scientific grant of ITME. Some of the numerical results were obtained using computer resources of the Interdisciplinary Centre for Mathematical and Computational Modelling (ICM), University of Warsaw.

References

1. A. Ortigosa-Blanch, J.C. Knight, W.J. Wadsworth, J. Arriaga, B.J. Mangan, T.A. Birks, P.St.J. Russell, Opt. Lett. **25**, 1325 (2000)
2. T.P. Hansen, J. Broeng, S.E.B. Libori, E. Knudsen, A. Bjarklev, J.R. Jensen, H. Simonsen, IEEE Photonics Technol. Lett **13**, 588 (2001)
3. K. Saitoh, M. Koshiba, IEEE Photonics Technol. Lett **14**, 1291 (2002)
4. M.J. Steel, T.P. White, C. Martijn de Sterke, R.C. McPhedran, L.C. Botten, Opt. Lett. **26**, 488 (2001)
5. O. Frazao, J. Santos, F. Araujo, L. Ferreira, Laser Photonics Rev. **2**, 449 (2008)
6. T. Martynkien, M. Szpulak, W. Urbanczyk, Appl. Opt. **44**, 7780 (2005)
7. M.J. Steel, R.M. Osgood Jr., Opt. Lett. **26**, 229 (2001)
8. T.L. Wu, C.H. Chao, IEEE Photonics Techol. Lett. **16**, 126 (2004)
9. N.J. Florous, M. Koshiba, J. Lightw. Technol. **23**, 1763 (2005)
10. Y.C. Liu, Y. Lai, Opt. Express **13**, 225 (2005)
11. Y. Yue, G. Kai, Z. Wang, T. Sun, L. Jin, Y. Lu, C. Zhang, J. Liu, Y. Li, Y. Liu, S. Yuan, X. Dong, Opt. Lett. **32**, 469 (2007)
12. D. Mogilevtsev, J. Broeng, S.E. Barkou, A. Bjarklev, J. Opt. A, Pure Appl. Opt. **3**, 141 (2001)
13. W. Zhi, R. Guobin, L. Shuqin, J. Shuisheng, Opt. Express **11**, 1966 (2003)
14. M.Y. Chen, R.J. Yu, J. Opt. A, Pure Appl. Opt. **3**, 512 (2004)
15. P. Szarniak, R. Buczynski, D. Pysz, I. Kujawa, M. Franczyk, R. Stepien, Proc. SPIE **5950**, 59501L (2005)
16. J. Wang, C. Jiang, W. Hu, M. Gao, H. Ren, Opt. Laser. Technol. **39**, 913 (2007)
17. N. Issa, M. van Eijkelenborg, M. Fellew, F. Cox, G. Henry, M. Large, Opt. Lett. **29**, 1336 (2004)
18. A. Bjarklev, J. Broeng, A.S. Bjarklev, *Photonic Crystal Fibres* (Kluwer Academic, Dordrecht, 2003)
19. M. Antkowiak, R. Kotynski, T. Nasilowski, P. Lesiak, J. Wojcik, W. Urbanczyk, F. Berghmans, H. Thienpont, J. Opt. A, Pure Appl. Opt. **7**, 763 (2005)
20. E. Silvestre, M.V. Andres, P. Andres, J. Lightw. Technol. **16**, 923 (1998)